

Thermally Stratified Magnetohydrodynamic Hybrid Williamson Nanofluid Flow in a Porous Medium Through a Vertical Cylinder

Jintu Mani Nath ^{1,*} , Ashish Paul ², Tusar Kanti Das ³

¹ Department of Mathematics, Mangaldai College, Mangaldai-784125, India; jmnath1995@gmail.com;

² Department of Mathematics, Cotton University, Guwahati-781001, India; ashish.paul@cottonuniversity.ac.in;

³ Department of Mathematics, Dudhnoi College, Dudhnoi-783124, India; tusarkantidas1995@gmail.com;

* Correspondence: jmnath1995@gmail.com (J.M.N.);

Scopus Author ID 57788867600

Received: date; Accepted: date; Published: date

Abstract: This present analysis intends to critique the thermally stratified magnetohydrodynamics (MHD) Williamson hybrid nanofluid stream across a linearly elongated vertical cylinder in a porous medium. Also, an inclined magnetic field along the stretching vertical cylinder is applied. A numerical solution for momentum and energy equations is obtained using MATLAB's Bvp4c methodology. The impact of different non-dimensional factors on velocity and thermal profile is portrayed graphically. Also, the expression of shear and thermal transmit rate are computed and demonstrated through the tables. This study is also motivated by the intention to strengthen our understanding of the mechanisms behind heat transport enhancement in non-Newtonian fluids. The basic novelty is to analyze how the rate of thermal transport is influenced by the conversion of Cu-ethylene glycol Williamson nanofluid to Cu-MoS₂/ethylene glycol Williamson hybrid nanofluid in the existence of a heat stratification. It has been found that the thermal curve is a reducing function of the thermal stratification factor. Meanwhile, there is notable heat stratification; the temperature turns negative, and it has been established that the Williamson hybrid nanofluid has a heat transmission rate higher than that of the Williamson nanofluid. The heat transmission speed increases by more than 13.3% for the Williamson hybrid nanofluid compared with the Williamson nanofluid. Also, the absolute value of the shear stress rate for the Williamson hybrid nanofluid is raised by up to 26.7% when contrasted with the Williamson nanofluid. This investigation has tremendous possibilities for optimizing heat transport in an assortment of industry-related uses, making it a vital addition to the fields of fluid mechanics and nanofluid technology research. Good agreement is noted throughout the outcomes and previously published work.

Keywords: hybrid nanofluid; stretched vertical cylinder; Williamson fluid; thermal stratification; volume concentration.

Nomenclature: $(C_p)_f$ = fluid specific heat capacity ($J kg^{-1}K^{-1}$); $(C_p)_{hnf}$ = hybrid nanofluid specific heat capacity ($J kg^{-1}K^{-1}$); $(C_p)_{s1}$ = specific heat capacity of the MoS₂ ($J kg^{-1}K^{-1}$); $(C_p)_{s2}$ = specific heat capacity of the Cu ($J kg^{-1}K^{-1}$); Gr_x = grashof number; k_f = fluid's thermal conductivity ($Wm^{-1}K^{-1}$); k_{bf} = nanofluid's thermal conductivity ($Wm^{-1}K^{-1}$); k_{hnf} = thermal conductivity of hybrid nanofluid ($Wm^{-1}K^{-1}$); k_{s1}, k_{s2} = solid nanoparticle's thermal conductivity ($Wm^{-1}K^{-1}$); k_p = permeability of porous media (m^2); M = magnetic parameter; P = porosity parameter; Pr = prandtl number; Re_x = local reynolds number; T = temperature of the fluid (K); T_∞ = fluid's surroundings temperature (K); T_w = wall temperature (K); w = the element of velocity in the r-direction (ms^{-1}); v = the element of velocity in the x directions (ms^{-1}); B_0 = magnetic field strength ($Nm^{-1}A^{-1}$); $(\beta_T)_f$ = fluid's thermal expansion (K^{-1}); $(\beta_T)_{s1}$ = thermal expansion of the MoS₂ (K^{-1});

$(\beta_T)_{s_2}$ =thermal expansion cu (K^{-1}); γ =the curvature parameter; δ =thermal stratification parameter; η =similarity variable; λ =thermal buoyancy parameter; μ_f =dynamic viscosity of the fluid (mPa); μ_{hnf} =dynamic viscosity of hybrid nanofluid (mPa); σ_{hnf} =hybrid nanofluid's electric conductivity ($Ohm^{-1}m^{-1}$); ρ_f =fluid's density (kgm^{-3}); ρ_{hnf} =hybrid nanofluid's density (kgm^{-3}); ρ_{s_1} =density of MoS_2 (kgm^{-3}); ρ_{s_2} =the density of Cu (kgm^{-3}); ϕ_1, ϕ_2 =the volume fraction of MoS_2 and Cu ; ψ =stream function; We =weissenberg number.

© 2025 by the authors. This article is an open-access article distributed under the terms and conditions of the Creative Commons Attribution (CC BY) license (<https://creativecommons.org/licenses/by/4.0/>).

1. Introduction

In thermal management, conventional fluids like water and oil are often utilized. Heat transmission efficiency is escalated by nanofluids, fluids that have been combined with nanoparticles to improve their thermal attributes. With better performance than traditional fluids, they are used in refrigeration systems, electronics, automobiles, and industrial processes. Additionally, relevant literature [1-7] contributed supplementary insights into significant research efforts within this domain.

A new kind of fluid that can provide significant thermal transmission for various manufacturing sectors is required due to the advancement of nanotechnology. In light of this, a novel fluid called a hybrid nanofluid was developed. Numerous researchers have broadened their computational and experimental work as a result of the recent discovery of hybrid nanofluid. A hybrid nanofluid can be produced by dispersing various kinds of nanoparticles in one or more base fluids. Hybrid nanofluids exhibit superior thermal features when contrasted with traditional nanofluids and base fluids. Applications for these fluids include freezing, generator cooling, automobile field, electronic cooling process, air conditioning, exchangers of heat, therapeutic uses, and nuclear system freezing.

The thermal transmission improvement in hydro-magnetic water-based Al_2O_3 -Cu hybrid nanofluid flow through a stretched cylinder was denominated by Maskeen *et al.* [8]. They demonstrated that compared to conventional fluids or nanofluids based on single nanoparticles, hybrid nanofluids are more efficient at transmitting heat. Manjunatha *et al.* [9] explored the thermal transport escalation in the boundary layer movement of hybrid nanofluids due to varying viscosity and natural convection. Subsequently, Khashi'ie *et al.* [10] sought out the movement of a hybrid nanofluid at its stagnation point through a porous longitudinal cylinder exhibiting an influence on heat stratification. In contrast with Cu- Al_2O_3 /water hybrid nanofluids, Al_2O_3 -water nanofluid functioned at an inferior thermal transfer rate throughout their study within a contracting cylinder.

Furthermore, the consequence of a hybrid nanofluid on the behavior of the boundary layer throughout a spinning cylinder was explored quantitatively by Elsaid *et al.* [11]. Also, in a permeable vertical cylinder with an inconsistent heat sink/source, Khan *et al.* [12] analyzed the mixed convective radiative flow generated by the hybrid nanofluid. They concluded that the radiation and curvature factors both boost the drag force. Mandal *et al.* [13] addressed the thermo-fluidic movement procedure in a novel M-shaped cavity packed with non-Darcian porous medium and hybrid nanofluid. Also, Biswas *et al.* [14] investigated the hybrid nanofluid-filled walled tilted permeable enclosure imposing a partially active magnetic field. Furthermore, Mandal *et al.* [15] explored the MHD Hybrid nanofluid combined convection in a novel W-shaped porous system.

The most challenging area of research over the past few years has been the investigation of fluid flow through stretched cylinders with their numerous characteristics. This occurrence profoundly affects technological and industry practices like polymer extruders, synthetic fiber manufacture, water distribution systems, copper wire manufacturing, and metal extrusion, among others. Crane [16] earliest penetrated the flow of the boundary layers triggered by a stretching cylinder. After that, the trajectory of a viscous fluid continuing through a stretched, hollow cylinder was investigated by Wang [17]. Takhar *et al.* [18] researched the mixed heat and mass transport via a vertically moving cylinder incorporating a free stream. Furthermore, Rashad *et al.* [19] investigated the mixed convection boundary-layer nanofluid flow past a horizontal circular cylinder embedded in a porous medium under convective boundary limitations.

Recently, Waqas *et al.* researched the mechanism of heat conduction in a magnetized motion of hybrid nanofluids throughout a vertically extended cylinder [20]. They established that the elevated magnitude of the porosity term minimizes fluid stream while boosting the thermal curve. Also, Sreenivasa *et al.* [21] conducted a computational investigation to determine the process of heat transport incorporating the transmission of ferromagnetic hybrid nanofluids through an extending cylinder.

Non-Newtonian fluids' flow and heat transmit features are significant to numerous and diverse biotechnology, pharmacology, and chemical engineering systems, among other disciplines. Therefore, despite its complexity, applied mathematicians and engineers concentrate on it. The study and utilization of non-Newtonian fluids, such as Williamson fluid, a component of the pseudo-plastic fluid family, are developing in several industrial and engineering applications, including blood circulation, aesthetic color-coated sheets, outer plates of polymers, etc. Williamson introduced the Williamson fluid during his groundbreaking study on the flow of pseudo-plastic materials in 1929. He spoke in depth about the pseudo-plastic materials before putting out a model to describe their flow, which was later confirmed through experiments. This model is currently referred to as the Williamson fluid model. Using nanomaterials, Hamid *et al.* [22] researched the influence of heat radiation on Williamson fluid flow caused by an expanding or constricting cylinder. After that, Khan *et al.* [23] analyzed how heat and solute stratification interfere with the viscosity of Williamson nanofluid flow. They established that the velocity curve decreases for high values of varying viscosity and heat stratification factors, while the heat stratification factor indicates reverse behavior for the thermal curve.

Furthermore, in evaluating sheet and cylinder on MHD convective flow, Hussain *et al.* [24] sought out the Williamson fluid featuring homogeneous-heterogeneous interactions. The findings demonstrate that liquid concentration and movement are more notable by cylinder than sheet. Bilal *et al.* explored Williamson nanofluid flow within a partially gliding and convective cylinder containing radiant heat and changing conductivity [25]. You *et al.* [26] investigated the series outcomes of three-dimensional MHD hybrid nanofluid flow and thermal transmission.

Researchers have thoroughly investigated heat and solute stratification's role in transporting heat and mass. In flow fields, stratification can be a result of variations in liquid density, concentration, or temperature. The process of thermal stratification is applied to groundwater aquifers, lake thermo-hydraulics, seismic fluxes, and salinity. Bilal *et al.* [27] computationally examined the thermally stratified Williamson fluid stream across a cylindrical domain through the Keller box approach. The findings illustrate that the thermal transmission

rate exhibits notable improvement for climbing magnitudes Prandtl number for cylindrical geometry rather than plane geometry. Optimization of heat and solutal stratification in the simulation of Williamson fluid incorporating entropy creation and activation energy was explored by Khan *et al.* [28]. Moreover, intending to figure out the radiative ethylene glycol-based bi-nanofluid flow on a curved surface underneath slip and heat stratified constraints, Ramzan *et al.* [29] performed a numerical simulation. They reported that stronger estimates of the stratification parameter are associated with a drop in temperature. A bio-convective hybrid nanofluid including triple stratification impacts was investigated for flow and thermal transmission by Khan *et al.* [30]. The impact of thermal stratification and radiation on a hybrid graphene oxide-Ag/H₂O nanofluid was addressed by Masood *et al.* [31]. Manzoor *et al.* [32] centered on the heat stratification and uneven thermal radiation in the Darcy-Forchheimer propagation of hybrid nanofluid by a spinning disc. Their findings show that the porosity factor and Reynolds number have positive magnitudes for velocity. In Williamson nanofluid, the stratified thermos-solutal Marangoni bioconvective flow of gyrotactic microorganisms was explored by Kairi *et al.* [33]. Moreover, various explorations [34-38] delved into distinct flow phenomena noticed in hybrid nanofluids over various constraints, enriching the understanding of this multifaceted region.

This investigation provides a relatively unexplored area of non-Newtonian fluid dynamics, concentrating on MoS₂-Cu/Ethylene glycol Williamson hybrid nanofluid movement via a vertical stretched cylinder subjected to free convection and thermal stratification. The flow problem also integrates the implication of an angled magnetic field. Nobody has investigated the Williamson hybrid nanofluid's flow incorporating heat stratification's influence on a linearly stretched vertical cylinder. This provides a significant research gap in the study. So, the present investigation is motivated by this, and the study of this phenomenon has a vast scope in the area of fluid dynamics. The primary novelty is to investigate how the rate of heat transport is influenced by the conversion of Cu-ethylene glycol Williamson nanofluid to Cu-MoS₂/ethylene glycol Williamson hybrid nanofluid in the existence of a heat stratification. This research is also inspired by the intention to strengthen our understanding of the mechanisms behind thermal transport augmentation in non-Newtonian fluids. In light of real-world applications requiring thermal transfer improvement, this study aims to expand understanding of the complex interactions between various components influencing fluid flow and heat transfer in non-Newtonian fluids. Practical applications of the research include the production of goods, thermal engineering, and energy generation—all domains where effective heat transportation is essential. Understanding how nanofluids' composition affects heating rates may help develop superior thermal transfer fluids and systems, which will increase the effectiveness and efficiency of thermal management practices in these industries. The governing set of nonlinear PDEs has been transfigured into a set of ODEs by employing an appropriate similarity transformation. To solve the nonlinear ODE system, Bvp4c [46] techniques are employed. Tabulated statistics are used to represent and compare numerous factors visually.

2. Mathematical Formulation

Consider a two-dimensional, steady Williamson hybrid nanofluid past through a stretched linear permeable vertical cylinder. The coordinate system used in this flow problem is cylindrical polar(x, r), where x and r signify along the axial and radial direction, respectively. The magnetic field has strength B_0 is exerted at an inclination, ξ to the vertical

direction. The thermal buoyancy consequence is also adopted in the momentum equation. Incorporating the surface velocity, $w_w = a \left(\frac{x}{l}\right)$, in tandem with its axis, the cylinder expands linearly, where a and l denote the velocity and characteristic length of the cylinder. $T_w(x) = T_0 + E \left(\frac{x}{l}\right)$ is considered to be wall temperature and $T_\infty(x) = T_0 + F \left(\frac{x}{l}\right)$ is the ambient temperature of the hybrid nanofluid, where E, F , and T_0 denote positive constants ($E > F$) and starting temperature, respectively.

Figure 1 indicates a schematic overview and coordinate system of the mathematical flow model.

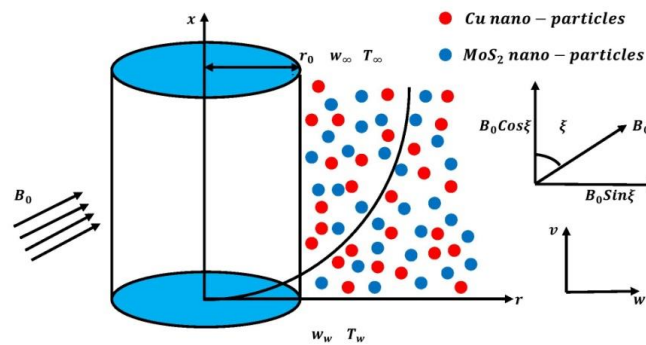


Figure 1. Pictorial demonstration of the flow model.

With these flow restrictions, the equations of the flow for Williamson hybrid nanofluid take the form [39-41]:

Continuity equation:

$$\frac{\partial(rw)}{\partial x} + \frac{\partial(rv)}{\partial r} = 0 \tag{1}$$

Momentum equation:

$$w \frac{\partial w}{\partial x} + v \frac{\partial w}{\partial r} = \frac{\mu_{hnf}}{\rho_{hnf}} \frac{1}{r} \frac{\partial}{\partial r} \left(r \frac{\partial w}{\partial r} \right) - \frac{\mu_{hnf}}{\rho_{hnf}} \left(\sqrt{2} \Gamma \frac{\partial w}{\partial r} \frac{\partial^2 w}{\partial r^2} + \frac{\Gamma}{\sqrt{2}} \frac{1}{r} \left(\frac{\partial w}{\partial r} \right)^2 \right) + \frac{(\rho\beta)_{hnf}}{\rho_{hnf}} g(T - T_\infty) - \frac{\sigma_{hnf}}{\rho_{hnf}} B_0^2 \cdot \text{Sin}^2 \xi \cdot w - \frac{\mu_{hnf}}{\rho_{hnf}} \frac{w}{k_p} \tag{2}$$

Energy equation:

$$w \frac{\partial T}{\partial x} + v \frac{\partial T}{\partial r} = \frac{k_{hnf}}{(\rho c_p)_{hnf}} \frac{1}{r} \frac{\partial}{\partial r} \left(r \frac{\partial T}{\partial r} \right) \tag{3}$$

The boundary constraints are:

$$\begin{aligned} w &= a \frac{x}{l}, \quad v = 0, \quad T = T_w(x) \quad \text{when } r = r_0 \\ w &= 0, \quad T \rightarrow T_\infty(x) \quad \text{when } r \rightarrow \infty \end{aligned} \tag{4}$$

The following variables ought to be utilized to account for similarity transformations [46]: [40]:

$$\eta = \frac{r^2 - r_0^2}{2r_0} \sqrt{\frac{a}{v_f l}}, \quad \psi = \sqrt{\frac{av_f}{l}} x r_0 f(\eta), \quad \theta = \frac{T - T_\infty(x)}{T_w(x) - T_0} \tag{5}$$

Where $w = \frac{1}{r} \frac{\partial \psi}{\partial r}$, $v = -\frac{1}{r} \frac{\partial \psi}{\partial x}$

Considering the aforementioned transformation, the reformed dimensionless nonlinear equations are outlined below:

$$f'^2 - f \cdot f'' = \left(\frac{\rho_f}{\rho_{hnf}} \frac{\mu_{hnf}}{\mu_f}\right) \{2\gamma f'' + (1+2\gamma\eta)f'''\} + \left(\frac{\rho_f}{\rho_{hnf}} \frac{\mu_{hnf}}{\mu_f}\right) \{3 \cdot We \cdot \gamma(1 + 2\gamma\eta)^{\frac{1}{2}} f''^2 + 2We(1 + 2\gamma\eta)^{\frac{3}{2}} f'' \cdot f'''\} + \left(\frac{\rho_f}{\rho_{hnf}} \frac{(\rho\beta)_{hnf}}{(\rho\beta)_f}\right) \lambda \cdot \theta - \left\{ \text{Sin}^2 \xi \cdot \left(\frac{\rho_f}{\rho_{hnf}} \frac{\sigma_{hnf}}{\sigma_f}\right) M + \left(\frac{\rho_f}{\rho_{hnf}} \frac{\mu_{hnf}}{\mu_f}\right) P \right\} f' \quad (6)$$

$$f'(\theta + \delta) - f\theta' = \left(\frac{k_{hnf}}{k_f} \frac{(\rho C_p)_f}{(\rho C_p)_{hnf}}\right) \left(\frac{1}{Pr}\right) \{2\gamma\theta' + (2\gamma\eta + 1)\theta''\} \quad (7)$$

The converted boundary constraints are as follows:

$$f'(0) = 1, \quad f(0) = 0 \\ \theta(0) = 1 - \delta, \quad f'(\infty) \rightarrow 0, \quad \theta(\infty) \rightarrow 0 \quad (8)$$

Where

$$M = \frac{B_0^2 l \sigma_f}{a \rho_f}, \quad P = \frac{l \vartheta_f}{a k_p}, \quad \gamma = \sqrt{\frac{l \vartheta_f}{a r_0^2}}, \quad \lambda = \frac{Gr_x}{Re_x^2}, \quad \delta = \frac{F}{E}, \quad Pr = \frac{\vartheta_f (\rho C_p)_f}{k_f}, \\ We = \frac{\Gamma a^{3/2} x}{\sqrt{2\nu l^{3/2}}}$$

The density ρ_{hnf} , heat conductivity k_{hnf} , thermal expansion $(\rho\beta)_{hnf}$, dynamic viscosity μ_{hnf} , thermal capacity $(\rho C_p)_{hnf}$ of hybrid nanofluid is indicated as follows[40-41]

$$\rho_{hnf} = (1 - \phi_2) \{ (1 - \phi_1) \rho_f + \phi_1 \rho_{s1} \} + \phi_2 \rho_{s2} \quad (9)$$

$$k_{hnf} = k_{bf} \left\{ \frac{k_{s2} + 2k_{bf} - 2\phi_2(k_{bf} - k_{s2})}{k_{s2} + 2k_{bf} + \phi_2(k_{bf} - k_{s2})} \right\} \quad (10)$$

$$\text{Where } k_{bf} = k_f \left\{ \frac{k_{s1} + 2k_f - 2\phi_1(k_f - k_{s1})}{k_{s1} + 2k_f + \phi_1(k_f - k_{s1})} \right\},$$

$$(\rho\beta)_{hnf} = (1 - \phi_2) \{ (1 - \phi_1) (\rho\beta)_f + \phi_1 (\rho\beta)_{s1} \} + \phi_2 (\rho\beta)_{s2} \quad (11)$$

$$\mu_{hnf} = \frac{\mu_f}{(1 - \phi_1)^{2.5} (1 - \phi_2)^{2.5}} \quad (12)$$

$$(\rho C_p)_{hnf} = (1 - \phi_2) \left\{ (1 - \phi_1) (\rho C_p)_f + \phi_1 (\rho C_p)_{s1} \right\} + \phi_2 (\rho C_p)_{s2} \quad (13)$$

Also, the friction drag and the heat transportation rate are determined by:

$$C_f Re_x^{1/2} = \frac{1}{(1 - \phi_1)^{2.5} (1 - \phi_2)^{2.5}} \left(f''(0) + \frac{We}{2} f''(0)^2 \right) \quad (14)$$

$$Nu_x Re_x^{-1/2} = -\frac{k_{hnf}}{k_f} \theta'(0) \quad (15)$$

3. Methodology

To deal with this, the dimensionless higher-order ODEs (6)– (7) are regenerated into an intermediate first-order boundary value problem incorporation with the associated related boundary impediments (8). MATLAB's well-known bvp4c strategy is utilized in conjunction with a shooting technique to encompass the aforementioned non-dimensional ODEs numerically. The bvp4c decoder provides precise outcomes by solving boundary value problems more precisely, even for intricate and chaotic formulations. Because of its resilient mesh enhancement function, the computing load is decreased, and the effectiveness of computation is increased. Meanwhile, an initial projection that fulfills the spatial constraints of the bvp4c solver is needed to use it. Bvp4c is the best approach for assessing the computational outcome of such non-dimensional complex ODEs; its convergence threshold is set at 10^{-4} .

4. Result and Discussion

This manuscript investigates the thermally stratified MHD Williamson MoS₂-Cu/ethylene glycol Hybrid nanofluid flow through a stretching vertical cylinder. Molybdenum disulfide (MoS₂) containing a 0.1 solid volume proportion is added onto the carrier fluid, ethylene glycol, then copper (Cu) nanoparticles featuring a 0.02 solid volume concentration to produce a hybrid nanofluid. This volume ratio remains fixed throughout the problem study. Ethylene glycol is utilized as a carrier fluid. Table 1 contains an outline of the fundamental fluid and the hybrid nanoparticle's thermo-physical features. The computational findings for the velocity and thermal distribution are evaluated utilizing the Bvp4c technique, which is a built-in feature of MATLAB. This study demonstrates a higher degree of accuracy of data than the previous ones. For comparison with previous research conducted by Ishak and Nazar [42], Elbashbeshy *et al.* [43], and Paul *et al.* [41], various outcomes for the rate of thermal transmission are listed in Table 2. It illustrates that the Bvp4c method is effective in obtaining numerical outcomes that are accurate and consistent with the findings of the other approaches.

Table 1. Thermo-physical features of fundamental fluid and nano-particles [41-45].

Thermo-physical features	ρ (Kg/m ³)	C_p (J/Kg K)	k (W/ mK)	σ (S/ m)	β (K ⁻¹)
MoS ₂	5060	397.21	904.4	2.09 x 10 ⁴	2.8424 x 10 ⁻⁵
Cu	8933	385	400	59.6 x 10 ⁶	1.67 x 10 ⁻⁵
C ₆ H ₂ O ₆	1109	2400	0.258	5.5 x 10 ⁻⁶	5.7 x 10 ⁻¹

Table 2. The associated findings of $-\theta'(0)$ with $M = P = \gamma = \delta = \lambda = We = \phi_1 = \phi_2 = 0$, $\xi = \frac{\pi}{2}$ and various values of Prandtl number [41-43].

Pr	Ishak and Nazar [42]	Elbashbeshy <i>et al.</i> [43]	Paul <i>et al.</i> [41]	Current study
1	1	1	1.0005	1
10	3.7207	3.7207	3.72	3.7207

Moreover, Table 3 also reported the systematic review of various experimental studies on the thermal transport phenomena of Cu and MoS₂-induced nanofluids. The cross-reference within the table exhibits that the thermal flux is significantly higher in the prepared nanofluids, and therefore, in each study carried out, is indicated as spitted out evidence in comparison between the two. The extracted studies confirm the high enhancement of thermal conductivity of the nanoparticles and convective heat transfer phenomena of the prepared Cu and MoS₂ nanofluidic. Based on the reviews within Table 3, it was noted that the existing data generally agrees with the current review that the addition of nanoparticles enhances the thermophysical capacity of the base fluids.

Table 3. Indication of greater heat transmission through some experimental investigation.

References	Nanoparticles involved	Type of Investigation	Outcomes
Suresh <i>et al.</i> [47]	Al ₂ O ₃ and Cu	Experimental	A stable hybrid nanofluid of 0.1% volume fraction enhances the thermal transport through the heated circular tube.
Zhang <i>et al.</i> [48]	MoS ₂	Experimental	The experimental findings indicate that the addition of nanoparticles in the palm oil-driven base fluid produced the best lubricating property. Moreover, a 6% mass fraction was identified to be the optimal addition concentration for MoS ₂ nanoparticles.
Mousavi <i>et al.</i> [49]	ZnO, MoS ₂	Experimental	The pumping power and friction fraction was escalated by the incorporation of MoS ₂ nanoparticles.

Figure 2 portrays how the thermal stratification parameter impacted the thermal curve. Physically, the procedure of layering fluids at varying temperatures to create distinctive layers based on temperature gradients is referred to as thermal stratification. The thermal curve reduces as heat stratification climbs. Furthermore, the fluid encircling the cylinder can be colder than the ambient whenever there is adequate heat stratification, triggering the temperature to drop. Deka *et al.* [44] claim that a strong stratification causes fluid movement to reverse across an infinite vertical cylinder. Our study found the same result for Cu/MoS₂-C₂H₆O₂ Williamson-hybrid-nanofluid flow.

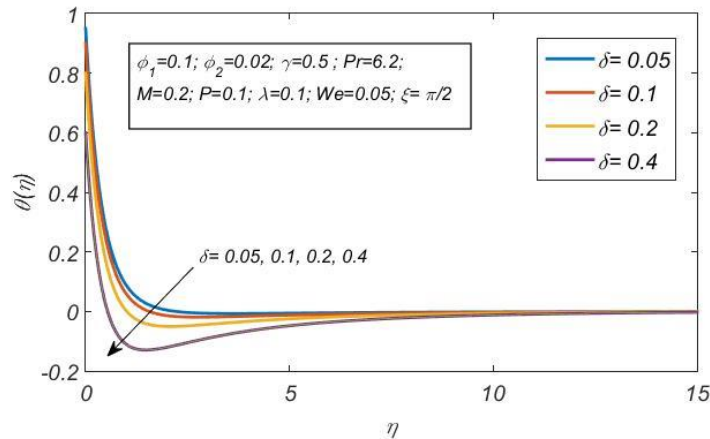


Figure 2. Demonstration of temperature against stratification parameter.

Figure 3 depicts the relationship between the fluid velocity and the Weissenberg number (*We*). Physically, the Weissenberg number is a dimensionless number that indicates the relative significance of elastic impacts to viscous influences in a flowing viscoelastic fluid, and it is clear that as the Weissenberg number increases, the velocity curve shrinks because rising Weissenberg number values enhance viscosity, which in turn improves resistance to fluid flow and lowers fluid velocity. Almaneea [26] also found the same outcomes for glycerin-driven Cu-Al₂O₃ MHD Williamson hybrid nanofluid. Figure 4 demonstrates how the thermal profile is impacted by the Weissenberg number. The Weissenberg number and temperature are directly connected. So, the thermal curve grows along with the Weissenberg number.

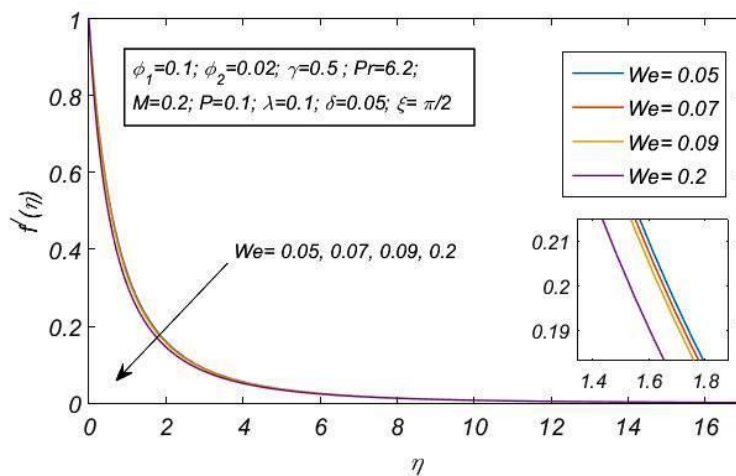


Figure 3. Demonstration on velocity against Weissenberg number.

Figures 5 and 6 show how the curvature term γ influences flow and the heat profile. It appears that fluid velocity escalates with increasing γ . As the radius of curvature drops as γ increases, the cylinder's circumference also reduces. As a consequence, fluid velocity

accelerates, and fluid particle impedance inside the cylinder is dwindled. Also, while the values of γ climb, the temperature curves rise. This result is similar to the investigation exhibited by Paul *et al.* [46] for using the Cu and Al₂O₃ nanoparticles.

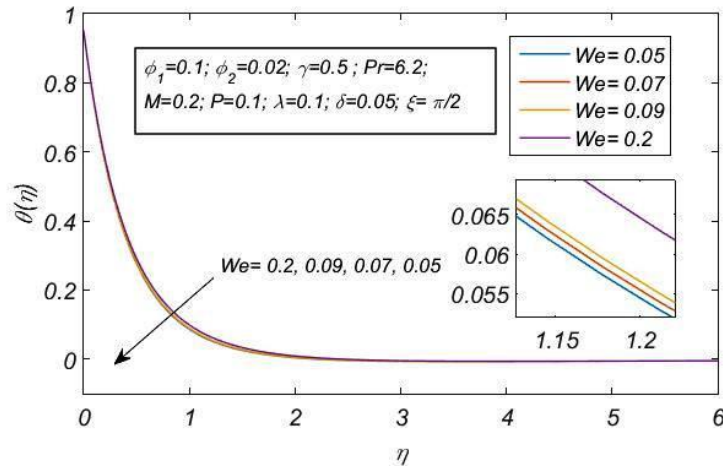


Figure 4. Demonstration on temperature against Weissenberg number

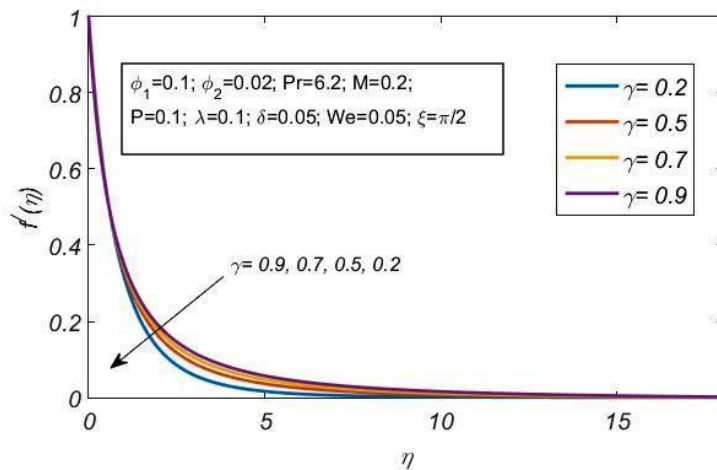


Figure 5. Demonstration on velocity against curvature term.

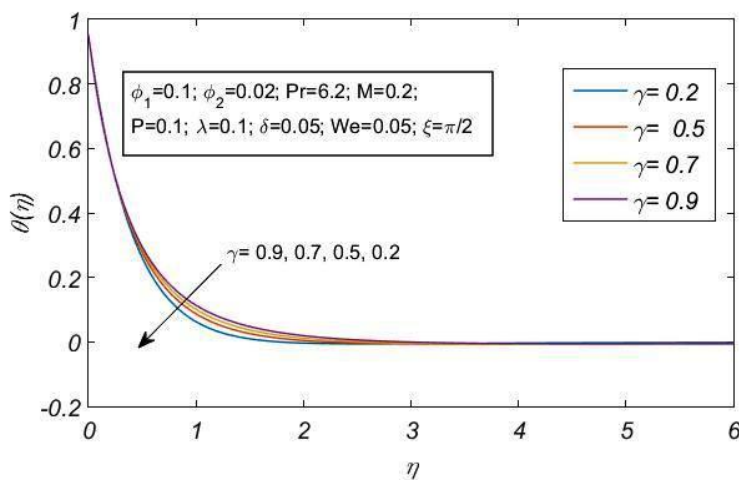


Figure 6. Demonstration on temperature against curvature term.

Figures 7 and 8 demonstrate the implication of the volume proportion of MoS₂ on both the velocity and thermal gradient curves while the volume fraction of Cu is fixed. It has been

reported that both the flow speed and the heat curve seem to be rising with an enhancement in the volume proportion of MoS₂ nanoparticles.

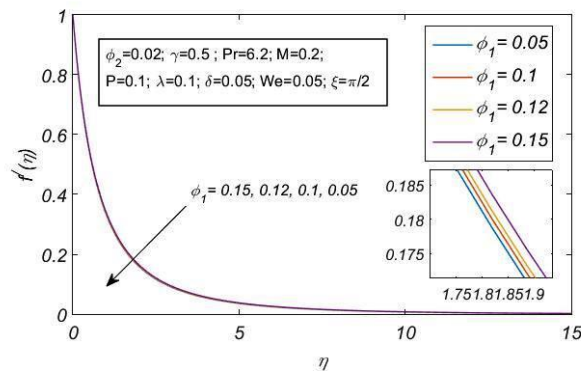


Figure 7. Illustration of volume fraction (ϕ_1) of MoS₂ on the velocity curve.

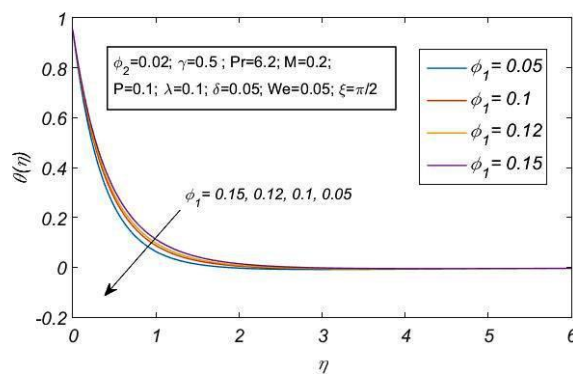


Figure 8. Illustration of volume fraction (ϕ_1) of MoS₂ on thermal profile.

In Table 4, the absolute shear rate and heat transmission rate are simulated numerically against distinct significant parameters like the Williamson factor, thermal stratification factor, and curvature factor when $\phi_1 = 0.1$ and $\phi_2 = 0.02$. An augmentation in the absolute value of the rate of friction drag and the rate of thermal transmission is noted with rising γ . Also, with growing values of We , and δ , the absolute value of the rate of shear stress is elevated. But a declination is noted in the rate of thermal transportation for rising We , and δ .

Table 4. Calculated skin-friction and Nusselt number values for varying magnitude of We, δ, γ when $\phi_1 = 0.1$ and $\phi_2 = 0.02$.

We	δ	γ	Skin-friction coefficient	Nusselt number
0.05	0.01	0.1	6.4256	5.9024
0.08			6.4575	5.8864
0.1			6.4820	5.8751
0.3			7.1353	5.7154
0.05	0.03	0.1	6.4275	5.8633
	0.08		6.4321	5.7656
	0.2		6.4432	5.5303
	0.4		6.4616	5.1365
	0.6		6.4800	4.7403
0.05	0.01	0.1	6.4256	5.9024
		0.5	7.5878	6.6069
		0.7	8.1343	6.9532
		1.2	9.4397	7.7988

Table 5 indicates that boosting the volume concentration of Cu nanoparticles whenever maintain $\phi_1 = 0$ leads to improvements in the absolute rate of shear and the Nusselt number. Furthermore, it has been established that the thermal transmit rate goes up by more than 13.3% when the volume fraction of MoS₂ is set to 0.1. The findings above demonstrate that the

Williamson hybrid nanofluid has a thermal transport rate that is undoubtedly greater than the Williamson nanofluid. Also, it has been shown that the absolute skin friction of the MoS₂-Cu/ethylene glycol Williamson hybrid nanofluid increased by more than 26.7%.

Table 5. Comparison of the skin friction coefficient and Nusselt numbers for Cu/C₆H₂O₆ Williamson-nanofluid and Cu-MoS₂/C₆H₂O₆ Williamson-hybrid- nanofluid

Cu/ethylene glycol				Cu- MoS ₂ /ethylene glycol			
$\phi_1(MoS_2)$	$\phi_2(Cu)$	Skin friction	Nusselt number	$\phi_1(MoS_2)$	$\phi_2(Cu)$	Skin friction	Nusselt number
0	0.02	1.4362	3.0649	0.1	0.02	1.8760	3.4595
	0.03	1.4909	3.1070		0.03	1.9363	3.5091
	0.04	1.5462	3.1496		0.04	1.9987	3.5592
	0.05	1.6023	3.1929		0.05	2.0618	3.6099
	0.09	1.8359	3.3702		0.09	2.3270	3.8186

5. Conclusion

The magnetohydrodynamic flow of Williamson MoS₂-Cu/ethylene glycol hybrid nanofluid over a linearly stretching vertical cylinder incorporating thermal stratification impact has been investigated computationally using the Bvp4c method. The inclined magnetic field is also taken into account in the flow mechanism. The pictorial demonstration of the effects of governing factors on the flow speed and temperature curves is also presented. The implications of those variables on the Nusselt term and the friction drag are also assessed.

The core findings of this study include that the temperature goes negative for ethylene glycol-driven MoS₂-Cu Williamson hybrid nanofluid when there is enough thermal stratification. Also, the Nusselt number is found to be lessened as the thermal stratification and Williamson parameters rise. It is also elevated as the curvature factor increases. Furthermore, the thermal curve goes up with the accelerated Weissenberg number and curvature parameter values. Also, a significant development in the velocity curve is noted with the boosting γ , but the retracted pattern is detected for We . The thermal transfer speed increases by more than 13.3% for MoS₂-Cu/ Ethylene glycol Williamson hybrid nanofluid when compared with Cu/ethylene glycol Williamson nanofluid. Williamson hybrid nanofluid has a heat transmission rate that is higher than that of Williamson nanofluid. The absolute value of the shear stress rate for MoS₂-Cu/ethylene glycol Williamson hybrid nanofluid is raised by up to 26.7% when contrasted with Cu/ethylene glycol Williamson nanofluid.

Several combinations of nanofluid and variable features like non-Newtonian behavior and heat generation can also be used for further study. Looking at nonlinear stretching surfaces, different magnetic field directions, and complex flow geometries can help to enhance understanding. The turbulent flow features can also be acquainted with the current flow geometry and several other complex geometries. The crucial step is to confirm these computational results experimentally. In addition, further research on transitory phenomena and practical applications in industrial cooling systems would help deepen the knowledge regarding those factors and offer practical examples for acting upon these findings. Another direction could be investigating the environmental impacts and sustainability of nanofluids.

Funding

This research received no external funding.

Acknowledgments

<https://nanobioletters.com/>

The authors acknowledge the Department of Mathematics, Cotton University, and the Department of Mathematics, Mangaldai College, for their valuable support and suggestions.

Conflicts of Interest

The authors declare no conflict of interest.

References

1. Chamkha, A. J.; Khaled, A. R. A. Hydromagnetic combined heat and mass transfer by natural convection from a permeable surface embedded in a fluid-saturated porous medium. *Int. J. Numer. Methods Heat Fluid Flow*. **2000**, *10*, 455-477, <https://doi.org/10.1108/09615530010338097>.
2. Chamkha, A. J. Coupled heat and mass transfer by natural convection about a truncated cone in the presence of magnetic field and radiation effects. *Numer. Heat Transfer Part A Appl*. **2021**, *39*, 511-530, <https://doi.org/10.1080/10407780120202>.
3. Chamkha, A. J.; Rashad, A. M. Natural convection from a vertical permeable cone in a nanofluid saturated porous media for uniform heat and nanoparticles volume fraction fluxes. *Int. J. Numer. Meth. Heat Fluid Flow*. **2012**, *22*, 1073-1085, <https://doi.org/10.1108/09615531211271871>.
4. Choudhury, R.; Dey, B.; Dasc, B. Hydromagnetic oscillatory slip flow of a visco-elastic fluid through a porous channel. *Chem. Eng*. **2018**, *71*, <https://doi.org/10.3303/CET1871161>.
5. Dey, B.; Kalita, B.; Choudhury, R. Radiation and chemical reaction effects on unsteady viscoelastic fluid flow through porous medium. *Frontiers in Heat and Mass Transfer (FHMT)*. **2022**, *18*, <https://doi.org/10.5098/hmt.18.32>.
6. Biswas, N.; Mandal, D. K.; Manna, N. K.; Gorla, R. S.; Chamkha, A. J. Hybridized nanofluidic convection in umbrella-shaped porous thermal systems with identical heating and cooling surfaces. *Int. J. Numer. Meth. Heat Fluid Flow*. **2023**, *33*, 3164-3201, <https://doi.org/10.1108/HFF-11-2022-0639>.
7. Halder, A.; Bhattacharya, A.; Biswas, N.; Manna, N. K.; Mandal, D. K. Convective heat transport and entropy generation in butterfly-shaped magneto-nanofluidic systems with bottom heating and top cooling. *Int. J. Numer. Meth. Heat Fluid Flow*. **2024**, *34*, 837-877, <https://doi.org/10.1108/HFF-06-2023-0353>.
8. Maskeen, M.M.; Zeeshan, A.; Mehmood, O.U.; Hassan, M. Heat transfer enhancement in hydromagnetic alumina-copper/water hybrid nanofluid flow over a stretching cylinder. *J. Therm. Anal. Calorim*. **2019**, *138*, 1127-1136, <https://doi.org/10.1007/s10973-019-08304-7>.
9. Manjunatha, S.; Kuttan, B. A.; Jayanthi, S.; Chamkha, A.; Gireesha, B. J. Heat transfer enhancement in the boundary layer flow of hybrid nanofluids due to variable viscosity and natural convection. *Heliyon*. **2019**, *5*, <https://doi.org/10.1016/j.heliyon.2019.e01469>.
10. Khashi'ie, N.S.; Hafidzuddin, E.H.; Arifin, N.M.; Wahi, N. Stagnation point flow of hybrid nanofluid over a permeable vertical stretching/shrinking cylinder with thermal stratification effect. *CFD Lett*. **2020**, *12*, 80-94.
11. Elsaid, E.M.; Abdel-wahed, M.S. Impact of hybrid nanofluid coolant on the boundary layer behavior over a moving cylinder: Numerical case study. *Case Stud. Therm. Eng*. **2021**, *25*, 100951, <https://doi.org/10.1016/j.csite.2021.100951>.
12. Khan, U.; Zaib, A.; Ishak, A.; Sherif, E.S.M.; Waini, I.; Chu, Y.M.; Pop, I. Radiative mixed convective flow induced by hybrid nanofluid over a porous vertical cylinder in a porous media with irregular heat sink/source. *Case Stud. Therm. Eng*. **2022**, *30*, 101711, <https://doi.org/10.1016/j.csite.2021.101711>.
13. Mandal, D. K.; Biswas, N.; Manna, N. K.; Gayen, D. K.; Gorla, R. S. R.; Chamkha, A. J. Thermo-fluidic transport process in a novel M-shaped cavity packed with non-Darcian porous medium and hybrid nanofluid: Application of artificial neural network (ANN). *Phys. Fluids*. **2022**, *34*, <https://doi.org/10.1063/5.0082942>.
14. Biswas, N.; Mondal, M. K.; Mandal, D. K.; Manna, N. K.; Gorla, R. S. R.; Chamkha, A. J. A narrative loom of hybrid nanofluid-filled wavy walled tilted porous enclosure imposing a partially active magnetic field. *Int. J. Mech. Sci*. **2022**, *217*, 107028, <https://doi.org/10.1016/j.ijmecsci.2021.107028>.

15. Mandal, D. K.; Biswas, N.; Manna, N. K.; Gorla, R. S. R.; Chamkha, A. J. Hybrid nanofluid magnetohydrodynamic mixed convection in a novel W-shaped porous system. *Int. J. Numer. Meth. Heat Fluid Flow*. **2023**, *33*, 510-544, <https://doi.org/10.1108/HFF-03-2022-0163>.
16. Crane, L.J. Boundary layer flow due to a stretching cylinder. *Z. Angew. Math. Phys.* **1975**, *26*, 619–622, <https://doi.org/10.1007/BF01594034>.
17. Wang, C.Y. Fluid flow due to a stretching cylinder. *Phys. Fluids* **1988**, *31*, 466–468, <https://doi.org/10.1063/1.866827>.
18. Takhar, H. S.; Chamkha, A. J.; Nath, G. Combined heat and mass transfer along a vertical moving cylinder with a free stream. *Heat Mass Transfer*. **2000**, *36*, 237-246, <https://doi.org/10.1007/s002310050391>.
19. Rashad, A. M.; Chamkha, A. J.; Modather, M. Mixed convection boundary-layer flow past a horizontal circular cylinder embedded in a porous medium filled with a nanofluid under convective boundary condition. *Comput. Fluids*. **2013**, *86*, 380-388, <https://doi.org/10.1016/j.compfluid.2013.07.030>.
20. Waqas, H.; Naqvi, S.M.R.S.; Alqarni, M.S.; Muhammad, T. Thermal transport in magnetized flow of hybrid nanofluids over a vertical stretching cylinder. *Case Stud. Therm. Eng.* **2021**, *27*, 101219, <https://doi.org/10.1016/j.csite.2021.101219>.
21. Sreenivasa, B.R.; Faqeeh, J.A.; Alsaiani, A.; Alzahrani, H.A.; Malik, M.Y. Numerical study of heat transfer mechanism in the flow of ferromagnetic hybrid nanofluid over a stretching cylinder. *Waves Random Complex Media* **2022**, 1–17, <https://doi.org/10.1080/17455030.2022.2061084>.
22. Hamid, A.; Khan, M.; Khan, U. Thermal radiation effects on Williamson fluid flow due to an expanding/contracting cylinder with nanomaterials: Dual solutions. *Phys. Lett. A* **2018**, *382*, 1982–1991, <https://doi.org/10.1016/j.physleta.2018.04.057>.
23. Khan, M.; Salahuddin, T.; Malik, M.Y.; Mallawi, F.O. Change in viscosity of Williamson nanofluid flow due to thermal and solutal stratification. *Int. J. Heat Mass Transf.* **2018**, *126*, 941–948, <https://doi.org/10.1016/j.ijheatmasstransfer.2018.05.074>.
24. Hussain, Z.; Hayat, T.; Alsaedi, A.; Ullah, I. On MHD convective flow of Williamson fluid with homogeneous-heterogeneous reactions: A comparative study of sheet and cylinder. *Int. Commun. Heat Mass Transf.* **2021**, *120*, 105060, <https://doi.org/10.1016/j.icheatmasstransfer.2020.105060>.
25. Bilal, M.; Siddique, I.; Borawski, A.; Raza, A.; Nadeem, M.; Sallah, M. Williamson magneto nanofluid flow over partially slip and convective cylinder with thermal radiation and variable conductivity. *Sci. Rep.* **2022**, *12*, 1–15, <https://doi.org/10.1038/s41598-022-16268-2>.
26. You, X.; Wang, Y. Series Solutions of Three-Dimensional Magnetohydrodynamic Hybrid Nanofluid Flow and Heat Transfer. *Nanomaterials* **2024**, *14*, 316, <https://doi.org/10.3390/nano14030316>.
27. Bilal, S.; Rehman, K.U.; Malik, M.Y. Numerical investigation of thermally stratified Williamson fluid flow over a cylindrical surface via Keller box method. *Results Phys.* **2017**, *7*, 690–696, <https://doi.org/10.1016/j.rinp.2017.01.032>.
28. Khan, M. I.; Qayyum, S.; Khan, T. A.; Khan, M. I.; Hayat, T.; Ullah, I.; Alsaedi, A. Optimization of thermal and solutal stratification in simulation of Williamson fluid with entropy generation and activation energy. *Heat Transf. Res.* **2019**, *50*, 865-882, <https://doi.org/10.1615/HeatTransRes.2018026342>.
29. Ramzan, M.; Gul, N.; Chung, J.D.; Kadry, S.; Chu, Y.M. Numerical treatment of radiative Nickel–Zinc ferrite-Ethylene glycol nanofluid flow past a curved surface with thermal stratification and slip conditions. *Sci. Rep.* **2020**, *10*, 1–14, <https://doi.org/10.1038/s41598-020-73720-x>.
30. Khan, M.N.; Ahmad, S.; Nadeem, S. Flow and heat transfer investigation of bio-convective hybrid nanofluid with triple stratification effects. *Phys. Scr.* **2021**, *96*, 065210, <https://doi.org/10.1088/1402-4896/abf305>.
31. Masood, S.; Farooq, M. Influence of thermal stratification and thermal radiation on graphene oxide-Ag/H₂O hybrid nanofluid. *J. Therm. Anal. Calorim.* **2021**, *143*, 1361–1370, <https://doi.org/10.1007/s10973-020-10227-7>.
32. Manzoor, U.; Muhammad, T.; Farooq, U.; Waqas, H. Investigation of thermal stratification and nonlinear thermal radiation in Darcy-Forchheimer transport of hybrid nanofluid by rotating disk with Marangoni convection. *Int. J. Ambient Energy* **2022**, 1–8, <https://doi.org/10.1080/01430750.2021.2023040>.
33. Kairi, R.R.; Roy, S.; Raut, S. Stratified thermosolutal Marangoni bioconvective flow of gyrotactic microorganisms in Williamson nanofluid. *Eur. J. Mech.-B/Fluids* **2023**, *97*, 40–52, <https://doi.org/10.1016/j.euromechflu.2022.09.004>.

34. Salahuddin, T.; Iqbal, M.A.; Bano, A.; Awais, M.; Muhammad, S. Cattaneo-Christov heat and mass transmission of dissipated Williamson fluid with double stratification. *Alexandria Eng. J.* **2023**, *80*, 553–558, <https://doi.org/10.1016/j.aej.2023.09.012>.
35. Farooq, U.; Waqas, H.; Makki, R.; Ali, M.R.; Alhushaybari, A.; Muhammad, T.; Imran, M. Computation of Cattaneo-Christov heat and mass flux model in Williamson nanofluid flow with bioconvection and thermal radiation through a vertical slender cylinder. *Case Stud. Therm. Eng.* **2023**, *42*, 102736, <https://doi.org/10.1016/j.csite.2023.102736>.
36. Alsallami, S.A.; Abbas, T.; Al-Zubaidi, A.; Khan, S.U.; Saleem, S. Analytical assessment of heat transfer due to Williamson hybrid nanofluid (MoS₂+ ZnO) with engine oil base material due to stretched sheet. *Case Stud. Therm. Eng.* **2023**, *51*, 103593, <http://dx.doi.org/10.1016/j.csite.2023.103593>.
37. Salahuddin, T.; Fatima, G.; Awais, M.; Khan, M.; Al Awan, B. Adaptation of nanofluids with magnetohydrodynamic Williamson fluid to enhance the thermal and solutal flow analysis with viscous dissipation: A numerical study. *Results Eng.* **2024**, *21*, 101798, <https://doi.org/10.1016/j.rineng.2024.101798>.
38. Farooq, U.; Safeer, M.; Cui, J.; Hussain, M.; Naheed, N. Forced convection analysis of Williamson-based magnetized hybrid nanofluid flow through a porous medium: Nonsimilar modeling. *Numer. Heat Transf. Part B Fundam.* **2024**, 1–17, <https://doi.org/10.1080/10407790.2023.2300704>.
39. Almaneea, A. Numerical study on heat and mass transport enhancement in MHD Williamson fluid via hybrid nanoparticles. *Alexandria Eng. J.* **2022**, *61*, 8343–8354, <https://doi.org/10.1016/j.aej.2022.01.041>.
40. Paul, A.; Nath, J.M.; Das, T.K. Thermally stratified Cu–Al₂O₃/water hybrid nanofluid flow with the impact of an inclined magnetic field, viscous dissipation and heat source/sink across a vertically stretching cylinder. *ZAMM-J. Appl. Math. Mech.* **2023**, *104*, e202300084, <https://doi.org/10.1002/zamm.202300084>.
41. Paul, A.; Mani Nath, J.; Kanti Das, T. An investigation of the MHD Cu–Al₂O₃/H₂O hybrid-nanofluid in a porous medium across a vertically stretching cylinder incorporating thermal stratification impact. *J. Therm. Eng.* **2023**, *9*, 1300847, <https://doi.org/10.18186/thermal.1300847>.
42. Ishak, A.; Nazar, R. Laminar boundary layer flow along a stretching cylinder. *Eur. J. Sci. Res.* **2009**, *36*, 22–29.
43. Elbashbeshy, E.M.A.; Emam, T.G.; El-Azab, M.S.; Abdelgaber, K.M. Laminar boundary layer flow along a stretching cylinder embedded in a porous medium. *Int. J. Phys. Sci.* **2012**, *7*, 3067–3072, <http://dx.doi.org/10.5897/IJPS12.093>.
44. Deka, R.K.; Paul, A. Transient free convection flow past an infinite moving vertical cylinder in a stably stratified fluid. *Trans. ASME J. Heat Transfer* **2012**, *134*, 0425031, <https://doi.org/10.1115/1.4005205>.
45. Unyong, B.; Vadivel, R.; Govindaraju, M.; Anbuviya, R.; Gunasekaran, N. Entropy analysis for ethylene glycol hybrid nanofluid flow with elastic deformation, radiation, non-uniform heat generation/absorption, and inclined Lorentz force effects. *Case Stud. Therm. Eng.* **2022**, *30*, 101639, <https://doi.org/10.1016/j.csite.2021.101639>.
46. Shampine, L.F.; Kierzenka, J.; Reichelt, M.W. Solving boundary value problems for ordinary differential equations in MATLAB with bvp4c. *Tutorial notes* **2000**, *2000*, 1–27.
47. Suresh, S.; Venkataraj, K. P.; Selvakumar, P.; Chandrasekar, M. Effect of Al₂O₃–Cu/water hybrid nanofluid in heat transfer. *Exp. Therm. Fluid Sci.* **2012**, *38*, 54–60, <https://doi.org/10.1016/j.expthermflusci.2011.11.007>.
48. Zhang, Y.; Li, C.; Jia, D.; Zhang, D.; Zhang, X. Experimental evaluation of MoS₂ nanoparticles in jet MQL grinding with different types of vegetable oil as base oil. *J. Clean. Prod.* **2015**, *87*, 930–940, <https://doi.org/10.1016/j.jclepro.2014.10.027>.
49. Mousavi, S. B.; Heris, S. Z.; Estellé, P. Viscosity, tribological and physicochemical features of ZnO and MoS₂ diesel oil-based nanofluids: An experimental study. *Fuel* **2021**, *293*, 120481, <https://doi.org/10.1016/j.fuel.2021.120481>.